Supporting Information

Conduction band photonic trapping via band gap reversal of brookite quantum dots using controlled graphitization for tuning a multi-exciton photoswitchable high-performance semiconductor

Varsha Khare[1], Aniket Kumar[2], Tae Woo Lee[3], Soo-Kyung Hwang[4], Piotr Jablonsky[5], Sangi-im Lee[6] and Sanjiv Sonkaria[1]**

AUTHOR ADDRESS

[1]Soft Foundry Institute, College of Engineering, Seoul National University, Seoul, Republic of Korea

[2]Innovoja Sustainable Solutions, White Rock, BC, Canada

[3]Department of Materials Science and Engineering, Seoul National University, Seoul, Republic of Korea

[4]Laboratory of Adhesion & Bio-Composites, Major in Environmental Materials Science, Seoul National University, Republic of Korea

[5]Laboratory of Behavioral Ecology, School of Biological Sciences, Seoul National University, Seoul, Republic of Korea

[6]Laboratory of Integrative Animal Ecology, Daegu Gyeongbuk Institute of Science and Technology (DGIST), South Korea

Supporting Figures

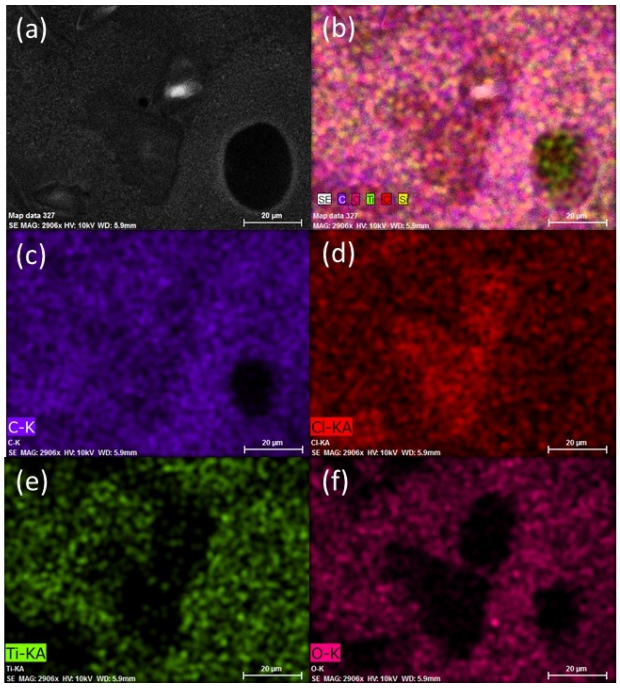

Figure S1: (a) The scanning electron microscopy image of rGO-brookite representative of the (b) overall elemental composition revealed by energy dispersive x-ray spectroscopy (EDX) showing the elemental distribution of (c) carbon (d) chlorine (e) titanium and (f) oxygen.

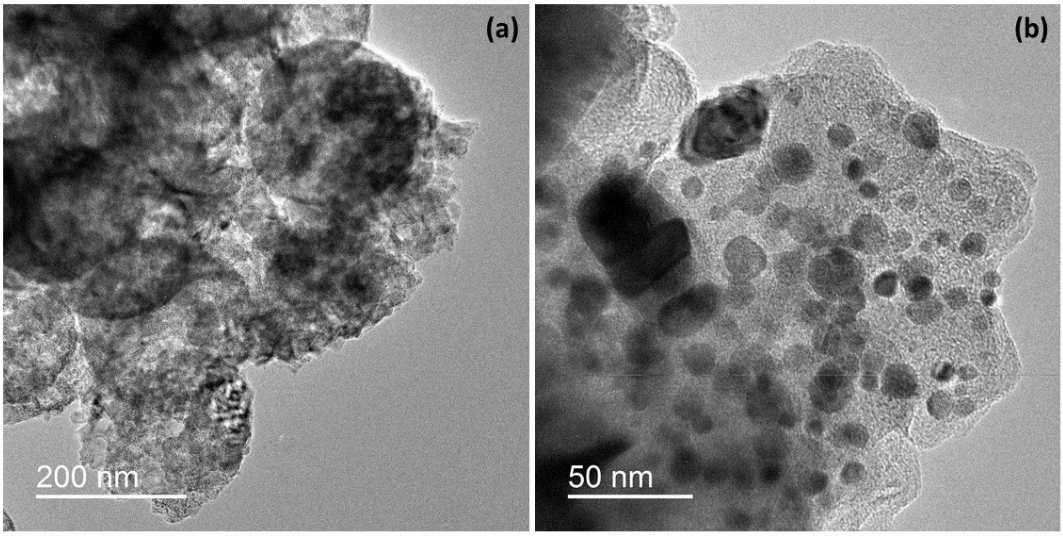

Figure S2: (a) Transmission electron microscopy imaging showing the morphogenesis of rGO-brookite particles from an amorphous origin. (b) Enlarged view of the detachment of particles depicting slowed nucleation and crystallised growth perturbed by the amorphous rGO network.

Supplementary text to the discussion on chemical fuels

Since pathways 1 and 2 are independent (shown in Scheme 2), the absence of a continuous energy dissipative process suggests that the coupling of monomers [M] into complexs [M*] and [M_2*] originate from atleast two different pathways to self-assembly (Scheme 2). The probable event which establishes the kinetic and thermodynamic stability of 'far-from-equilibrium' structures is the utilisation of released chemical fuel (F) from waste (W) accompanying [M*] and [M_2*] during the re-structuring of elemental building blocks. The energetic feasibility in driving the self of non-equilibrium structures is determined by the chemical potential which equates to the energy difference between (M + F) and (M + W) or (M_2 + F) and (M_2 + W) eloquently described by das et al [39]. We identify the co-assembly of the oxidant di-chloro, di-cyano benzoquinone as the coupling factor between chemically fuelled pathways 1 and 2 driving a synergistic relationship between the intrinsic nature of the buildings blocks in their chemical connectivity and the energy exchange with the surroundings. This translates to the ability of the activated complex M* to form elaborative surface complexes as dimers and semi-dimers [M_2*] from monomers [M]. The availability of the chemical fuel is deterministic in negotiating energy barriers to polymer complexation and enabling the modulation of surface functionality. In this instance, it is preferable that consumed energy (–ΔG) of the chemical fuel is stored in the aggregation of dimeric conjugated structures strongly favouring the dissipation self-assembled building blocks from the chemical surroundings shifting away from equilibrium towards charge transfer within the semiconductor complex.

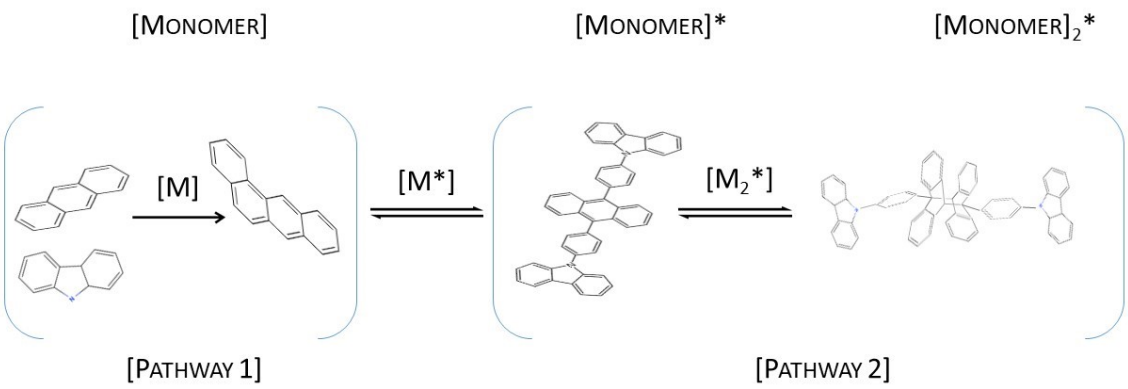

Scheme 2 Chemical fuel and chemical waste synergy in driving pathway progression favouring monomer self- assembly among closely related energy structures at the GO surface

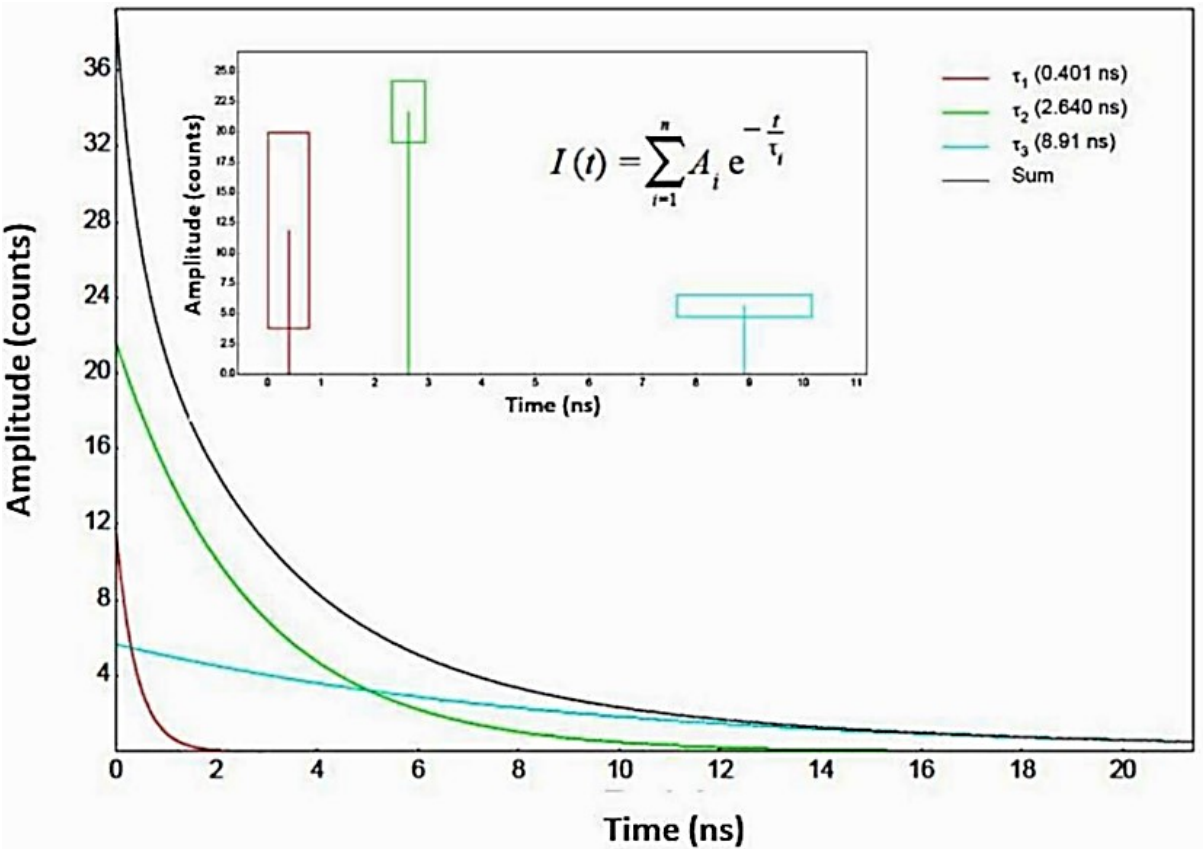

Figure S3: (a) Decay kinetics of rGO-brookite reflecting a mixed-transitory state under excitation characterised by decay constants τ_1, τ_2 and τ_3. transitory at the nanosecond scale in the photo-intensity range I5.3 corresponding PL peak 5.

Photon Intensity (peak Position in nm)	Decay times of peak 1									
	τ_1(ns)	%	τ_2(ns)	%	τ_3(ns)	%	τ_4(ns)	%	$\tau_{Av\text{-}Int}$(ns)	$\tau_{Av\text{-}Amp}$(ns)
5.3	—	—	—	—	—	—	—	—	—	—
5.5(305)	0.11	0.03	4.17	96.62	0.00	0.00	0.00	0.00	4.04	1.88
6 (301)	6.83	0.49	0.15	1.17	3.58	48.88	0.00	0.00	5.13	3.03
6.5 (303)	0.14	2.51	3.69	56.34	7.30	41.15	0.00	0.00	5.09	2.60
7(299)	7.51	44.82	2.59	39.42	0.50	7.04	9.63	8.72	6.14	2.81
Photon Intensity (peak Position in nm)	Decay times of peak 2									
	τ_1(ns)	%	τ_2(ns)	%	τ_3(ns)	%	τ_4(ns)	%	$\tau_{Av\text{-}Int}$(ns)	$\tau_{Av\text{-}Amp}$(ns)
5.3 (438)	0.69	7.06	4.08	6.50	11.32	33.05	87.00	3.39	5.36	2.87
5.5	—	—	—	—	—	—	—	—	—	—
6 (430)	2.74	40.39	0.60	6.99	7.64	43.65	18.86	8.98	6.17	3.06
6.5 (432)	2.37	35.77	0.45	5.94	6.95	47.27	18.22	11.02	6.17	2.80
7	—	—	—	—	—	—	—	—	—	—
Photon Intensity (peak Position in nm)	Decay times of peak 3									
	τ_1(ns)	%	τ_2(ns)	%	τ_3(ns)	%	τ_4(ns)	%	$\tau_{Av\text{-}Int}$(ns)	$\tau_{Av\text{-}Amp}$(ns)
5.3 (455)	6.31	2.72	1344.00	97.28	0.00	0.00	0.00	0.00	1307.73	198.39
5.5	—	—	—	—	—	—	—	—	—	—
6 (477)	0.71	6.08	3.06	35.12	8.36	44.28	18.54	14.52	7.51	3.83
6.5 (473)	—	—	—	—	—	—	—	—	—	—
7 (473)	2.30	26.76	0.46	3.11	6.60	48.04	16.30	22.08	7.40	3.69
Photon Intensity (peak Position in nm)	Decay times of peak 4									
	τ_1(ns)	%	τ_2(ns)	%	τ_3(ns)	%	τ_4(ns)	%	$\tau_{Av\text{-}Int}$(ns)	$\tau_{Av\text{-}Amp}$(ns)
5.3 (590)	4.48	23.89	185.30	76.11	0.00	0.00	0.00	0.00	142.08	17.40
5.5	—	—	—	—	—	—	—	—	—	—
6 (579)	3.68	49.03	0.47	2.55	8.77	46.27	27.34	2.15	6.46	4.15
6.5 (575)	0.52	3.67	2.39	26.59	6.58	47.03	16.14	22.72	7.42	3.74
7 (575)	8.33	55.02	3.32	39.47	0.42	2.54	26.67	2.97	6.69	4.06
Photon Intensity (peak Position in nm)	Decay times of peak 5									
	τ_1(ns)	%	τ_2(ns)	%	τ_3(ns)	%	τ_4(ns)	%	$\tau_{Av\text{-}Int}$(ns)	$\tau_{Av\text{-}Amp}$(ns)

5.3 (773)	**0.40**	**4.23**	**2.64**	**50.84**	**8.91**	**44.93**	**0.00**	**0.00**	**5.36**	**2.87**
5.5	—	—	—	—	—	—	—	—	—	—
6 (754)	**0.70**	**6.48**	**2.77**	**33.17**	**8.03**	**52.63**	**31.72**	**7.72**	**7.64**	**3.57**
6.5 (752)	**6.39**	**66.49**	**1.41**	**21.82**	**26.27**	**11.69**	**0.00**	**0.00**	**7.63**	**3.80**
7 (755)	**6.31**	**66.06**	**1.38**	**21.78**	**25.35**	**12.16**	**0.00**	**0.00**	**7.55**	**3.74**

Table S1: Summary of the multi-peak decay kinetics for rGO-brookite under variable photo-intensities.

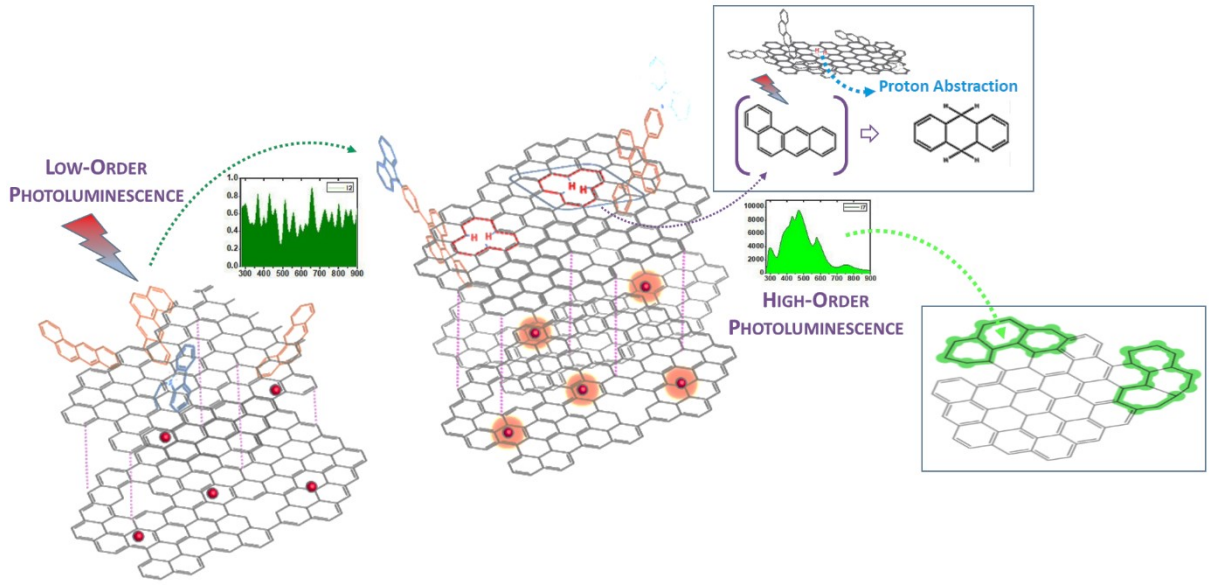

Figure S4: (a) A schematic rationalising the role of reduced graphene oxide following excitation inducing a high $e^- h^+$ separation at the rGO-brookite interface via proton abstraction and defect driven state.